

## Article

# Performance of TiB<sub>2</sub> Wettable Cathode Coating

Bo Yang<sup>1,2,†</sup>, Ruzhen Peng<sup>1,3,†</sup>, Dan Zhao<sup>1,†</sup>, Ni Yang<sup>1,4,†</sup>, Yanqing Hou<sup>1,\*</sup> and Gang Xie<sup>1,4,\*</sup>

<sup>1</sup> Faculty of Metallurgy and Energy Engineering, Kunming University of Science and Technology, Kunming 650093, China; yangbo@stu.kust.edu.cn (B.Y.); yxp@stu.kust.edu.cn (R.P.); zhaoddan@stu.kust.edu.cn (D.Z.); yqh@stu.kust.edu.cn (N.Y.)

<sup>2</sup> School of Materials and Civil Engineering, Guizhou Normal University, Guiyang 550014, China

<sup>3</sup> Department of Materials and Metallurgy Chemistry, Jiangxi University of Science and Technology, Ganzhou 341000, China

<sup>4</sup> Kunming Metallurgical Research Institute, Kunming 650093, China

\* Correspondence: hyqsimu@kust.edu.cn (Y.H.); wqs@stu.kust.edu.cn (G.X.)

† These authors contributed equally to this work.

**Abstract:** A TiB<sub>2</sub> wetttable cathode coating was deposited on a graphite carbon cathode material via atmospheric plasma spraying (APS). The microstructure and phase composition of the TiB<sub>2</sub> coating were analyzed via scanning electron microscopy (SEM), X-ray diffraction (XRD), and energy-dispersive X-ray spectroscopy (EDS). The wettability and corrosion resistance of the coating were studied in a molten-aluminum electrolytic system. The results showed that the surface of the TiB<sub>2</sub> coating prepared via plasma spraying was flat and that the main phase of the coating was TiB<sub>2</sub>. The wettability between the TiB<sub>2</sub> coating and liquid aluminum was better than that between graphite cathode carbon block and liquid aluminum. The abilities of the TiB<sub>2</sub> coating and graphite cathode carbon block to resist sodium (Na) penetration and prevent molten salt corrosion were compared through a corrosion test. The TiB<sub>2</sub> coating was found to have better resistance to Na penetration and better refractory cryolite corrosion resistance than graphite cathode carbon block.

**Keywords:** plasma spraying; TiB<sub>2</sub> wetttable cathode coating; wettability; corrosion resistance



**Citation:** Yang, B.; Peng, R.; Zhao, D.; Yang, N.; Hou, Y.; Xie, G.

Performance of TiB<sub>2</sub> Wettable Cathode Coating. *Minerals* **2022**, *12*, 27. <https://doi.org/10.3390/min12010027>

Academic Editors: Kenneth N. Han, Shuai Wang, Xingjie Wang and Jia Yang

Received: 4 November 2021

Accepted: 22 December 2021

Published: 24 December 2021

**Publisher's Note:** MDPI stays neutral with regard to jurisdictional claims in published maps and institutional affiliations.



**Copyright:** © 2021 by the authors. Licensee MDPI, Basel, Switzerland. This article is an open access article distributed under the terms and conditions of the Creative Commons Attribution (CC BY) license (<https://creativecommons.org/licenses/by/4.0/>).

## 1. Introduction

Currently, cryolite molten salt electrolysis is the only method for smelting aluminum [1]. During the electrolysis of molten cryolite, the cathode carbon block exhibits some corrosion properties; especially, sodium (Na) permeates into the cathode carbon block and causes the expansion of the carbon block, which is the main cause of the cathode damage and failure [2].

Many studies on cathodic carbon blocks have focused on wetttable cathodes, among which TiB<sub>2</sub> has become a research hotspot, because it is characterized by good wettability to liquid aluminum, low resolution, resistance to electrolyte erosion, and good electrical conductivity [3]. At present, many domestic and foreign studies on TiB<sub>2</sub> and its composites mainly focus on TiB<sub>2</sub> ceramic cathodes [4,5], TiB<sub>2</sub>-carbon adhesive coating [6–8], TiB<sub>2</sub> layer prepared by plating in molten salt [9–11], TiB<sub>2</sub> non-carbon adhesive coating [12], TiB<sub>2</sub> coating prepared via chemical vapor deposition [13], TiB<sub>2</sub> coating prepared via self-spreading high-temperature synthesis TiB<sub>2</sub> coating [14], and TiB<sub>2</sub> coating prepared via plasma spraying [15].

In recent years, our research group has conducted numerous studies on the TiB<sub>2</sub> coating preparation via atmospheric plasma spraying (APS) and has achieved certain results. Through several orthogonal experiments on spraying parameters, the best process conditions for the coating preparation have been obtained [16]. The influence of mechanical properties has been studied [17]. The current study mainly investigates the microstructure of TiB<sub>2</sub> coating prepared via APS under optimal process conditions and the wettability and corrosion resistance of TiB<sub>2</sub> coating in a molten-salt electrolytic aluminum system.

## 2. Materials and Methods

### 2.1. Materials

The TiB<sub>2</sub> powder used in the experiment was obtained from a certain chemical industry research institute in Shenyang (TiB<sub>2</sub> ≥ 98.5%), with a particle size of −325+400 mesh (38–45 μm). For aluminum electrolysis, a graphite cathode carbon block was adopted as the matrix (the specification was 100 mm × 100 mm × 30 mm); it was provided by an aluminum factory in Yunnan and needed to be polished and sandblasted in advance.

### 2.2. Preparation of Plasma-Sprayed TiB<sub>2</sub> Coating

During the TiB<sub>2</sub> coating preparation, first, the carbon block and TiB<sub>2</sub> powder were placed into the drying box and heated up to 100 °C for 4 h to remove the moisture, improve the TiB<sub>2</sub> powder fluidity, and improve the bonding strength between the carbon block and TiB<sub>2</sub> coating. Furthermore, TiB<sub>2</sub> powder was deposited on the graphite cathode carbon block using the DH-2080 plasma spray gun (Shanghai Ruifa Spraying Machinery Co., Ltd., Shanghai, China), with argon as the main gas, hydrogen as the secondary gas, and argon and hydrogen as the powder carrier gases. Before the preparation of the TiB<sub>2</sub> wettable cathode coating via spraying, the DH-2080 plasma spray gun was used to preheat the surface of the roughened and clean carbon block. The preheating temperature was maintained between 100 °C and 200 °C to shorten the temperature difference between the substrate and the TiB<sub>2</sub> powder and reduce the residual stress between the coating and the carbon block substrate. After the preheating, the plasma-spraying process parameters (Table 1) were adjusted, and the TiB<sub>2</sub> coating was sprayed on the carbon block substrate to obtain a TiB<sub>2</sub> coating with ~1000 μm thickness.

**Table 1.** Parameters of TiB<sub>2</sub> coating prepared via atmospheric plasma spraying (APS).

Name	Voltage	Current	Distance	Main Air Flow	Powder Feeding Rate	Ar Air Flow	Particle Diameter	Spray Gun Moving Speed
Parameter	72 V	550 A	90 mm	1800 L·h <sup>-1</sup>	27.34 g·min <sup>-1</sup>	120 L·h <sup>-1</sup>	(d <sub>50</sub> ) ≤ 37.4 μm	100 mm·s <sup>-1</sup>

### 2.3. TiB<sub>2</sub> Coating Characterization

The TiB<sub>2</sub> coating prepared via plasma spraying was peeled off from the base carbon block and then ground. The phase composition of the prepared TiB<sub>2</sub> coating powder was analyzed using the X'pert 3 powder-type diffractometer produced by PANalytical (Malvern, UK). The parameters were as follows: Cu target, acceleration voltage of 40 kV, current of 40 mA, and sweep speed of 8° min<sup>-1</sup>. After the TiB<sub>2</sub> cathode coating subjected to different treatments was polished with sandpaper, the coating surface was observed under a QUANTA600 scanning electron microscope to detect the microscopic internal structure of the coating. Moreover, energy spectrum analysis was performed using the NORAN SYSTEM SIX energy spectrometer (SelectScience, Bath, UK).

### 2.4. Method for Wettability Measurement

In this study, the wetting angle between the plasma-sprayed TiB<sub>2</sub> inert cathode coating and molten aluminum was not directly measured; only the wettability between the TiB<sub>2</sub> inert cathode coating and molten aluminum was qualitatively characterized. First, an appropriate number of aluminum ingots were placed in the silicon carbide crucible, and the silicon carbide crucible was placed in a resistance furnace, model RF-15-10, produced by Changsha Gongtai Experimental Electric Furnace Co., Ltd (Changsha, China), and the heating system was set to 750 °C. When the aluminum ingot in the silicon carbide crucible became molten, the plasma-sprayed TiB<sub>2</sub> cathode coating sample and the aluminum electrolytic cathode carbon block preheated at the same temperature were simultaneously immersed in the molten aluminum; the immersion time was 5 s. Subsequently, the sample was taken out from the molten aluminum and placed on a steel plate at 45 °C with the horizontal ground. After the molten aluminum on the surface of the sample was cooled,

aluminum was found to occur on the TiB<sub>2</sub> inert cathode coating and the carbon block. The spreading situations on the cathode and the wettability of the TiB<sub>2</sub> coating and carbon block were qualitatively evaluated.

### 2.5. Corrosion Resistance Test Method

Determination of the dissolution loss of TiB<sub>2</sub> coating in molten aluminum: The TiB<sub>2</sub> coating sample was soaked in high-temperature liquid aluminum at 960 °C for 48 h. After the molten aluminum sample was cooled, the change in the Ti content in the molten aluminum was analyzed, and then the dissolution loss of the TiB<sub>2</sub> coating in the molten aluminum was evaluated. The ARL841OX XRF was used to determine the titanium content in the liquid aluminum.

Static molten salt corrosion test of TiB<sub>2</sub> coating: The TiB<sub>2</sub> coating sample was placed on the bottom of a 0.5 L graphite crucible, and the prepared electrolyte (including Na<sub>3</sub>AlF<sub>6</sub>, NaF, Al<sub>2</sub>O<sub>3</sub>, and CaF<sub>2</sub> in mass percentages of 71.5%, 14.5%, 9.0%, and 5.0%, respectively) was added into a graphite crucible. The crucible was placed into a 960 °C atmosphere furnace and kept for 100 h. After the corrosion was over, the crucible was cooled to room temperature. Then, the TiB<sub>2</sub> coating sample at the bottom of the electrolytic cell was removed, and the residual electrolyte on the surface was cleaned. The sample was then cut along the central axis. Scanning electron microscopy (SEM) and energy-dispersive X-ray spectroscopy (EDS) were used to characterize the TiB<sub>2</sub> coating after static corrosion.

Static molten salt corrosion test of TiB<sub>2</sub> coating: The TiB<sub>2</sub> coating sample was placed on the bottom of a 0.5 L graphite crucible, and the prepared electrolyte (including Na<sub>3</sub>AlF<sub>6</sub>, NaF, Al<sub>2</sub>O<sub>3</sub>, and CaF<sub>2</sub> in mass percentages of 71.5%, 14.5%, 9.0%, and 5.0%, respectively) was added into the graphite crucible. The crucible was then placed into a 980 °C pit furnace. The graphite anode embedded in cast iron was inserted into the electrolytic cell. The area of the graphite anode was 28 cm<sup>2</sup>. After the electrolyte was melted, the current density was kept at 0.7 A·cm<sup>-2</sup>, and electrolysis was conducted for 4 h. The electrolyte was added to the electrolytic cell every 15 min. The subsequent treatment after electrolysis was the same as that in the static test.

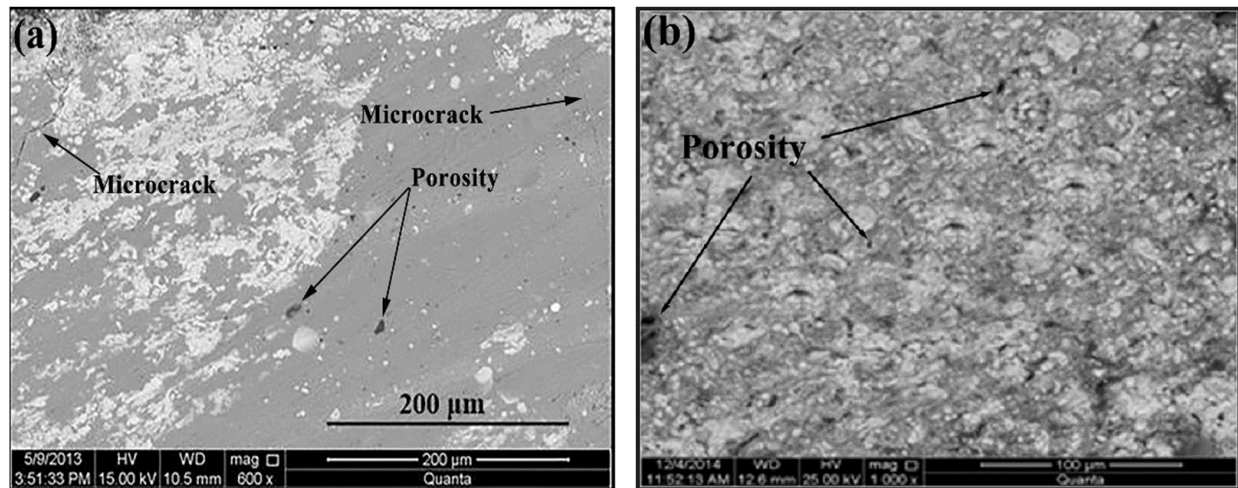
## 3. Results and Discussion

### 3.1. TiB<sub>2</sub> Coating Microstructure

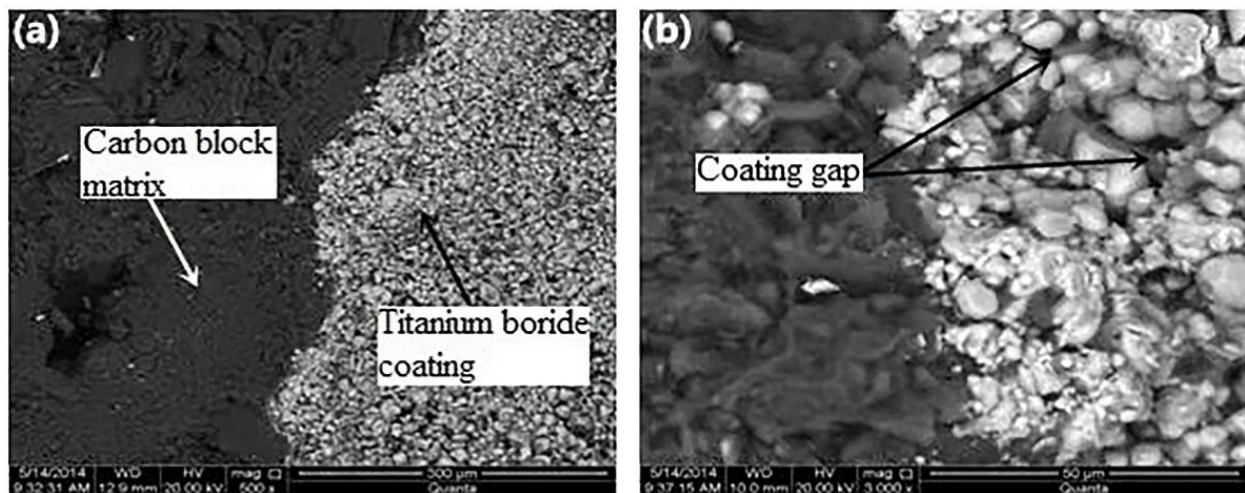
Figure 1a,b are the SEM images of the TiB<sub>2</sub> coating surface prepared via APS at two different magnifications. Figure 1a shows that the coating internal structure was relatively dense and uniformly distributed. The coating mainly showed two colors of dark gray and white. Moreover, small cracks occurred in the coating. The formation of such microcracks depends on the melting of TiB<sub>2</sub>, the volume shrinkage of the particles, and the TiB<sub>2</sub> coating cooling process. Figure 1b shows that after the TiB<sub>2</sub> powder was remelted and recrystallized, the particle size of the coating was not uniform. The distribution of such particles led to the generation of pores in the coating, and the increase in porosity will reduce the coating hardness and the bonding strength between the coating and the substrate; moreover, it will destroy the conductive network of the TiB<sub>2</sub> coating and increase the coating resistivity.

Figure 2a,b are the cross-sectional topography images of the TiB<sub>2</sub> coating under two different magnifications. The figure shows a clear boundary between the substrate and the coating. The gray area is the TiB<sub>2</sub> coating, and the black area is the carbon block substrate. The coating was formed by injecting TiB<sub>2</sub> powder into a high-temperature plasma jet and then transporting it to the substrate. The temperature at the center of the plasma flame was as high as 32,000 K, and the temperature at the nozzle outlet was still up to 20,000 K. The TiB<sub>2</sub> powder particles were instantly heated to a molten or semi-melted state in the high-temperature plasma jet. When the particles hit the carbon block substrate surface, they spread into a flat liquid covering and clung to the concave and convex points on the surface of the carbon block substrate. It shrank and bit the anchor point during condensation. Therefore, the combination of the TiB<sub>2</sub> coating and the carbon block substrate was mainly mechanical embedded-type. Because the TiB<sub>2</sub> coating was formed by solidifying a single

particle as a unit to the substrate surface in a layered accumulation, the difference in particle size between the droplets resulted in some voids in the coating. Moreover, it can be seen from the cross section of the coating that the substrate and the coating. The bonding interface of the layer was clear, smooth, and tortuous, which shows that the coating was tightly bonded.



**Figure 1.** Scanning electron microscopy (SEM) image of  $\text{TiB}_2$  coating surface morphology. (a) SEM of coating under 600 times, (b) SEM of coating under 1000 times.



**Figure 2.**  $\text{TiB}_2$  coatings sectional SEM micrographs. (a) SEM of coating under 600 times, (b) SEM of coating under 1000 times.

### 3.2. X-ray Diffraction Pattern of $\text{TiB}_2$ Coating

Figure 3 is the X-ray diffraction (XRD) analysis result of the  $\text{TiB}_2$  coating prepared via APS. The figure shows that the coating was mainly composed of  $\text{TiB}_2$ ,  $\text{TiO}_2$ , and a small amount of  $\text{B}_2\text{O}_3$ , indicating that  $\text{TiB}_2$  was oxidized during the spraying process. This was mainly due to the air involved in the plasma jet and the molten  $\text{TiB}_2$  particles during the plasma-spraying process. Contact causes  $\text{TiB}_2$  particles to be oxidized to form oxidation products such as  $\text{TiO}_2$  and  $\text{B}_2\text{O}_3$ .

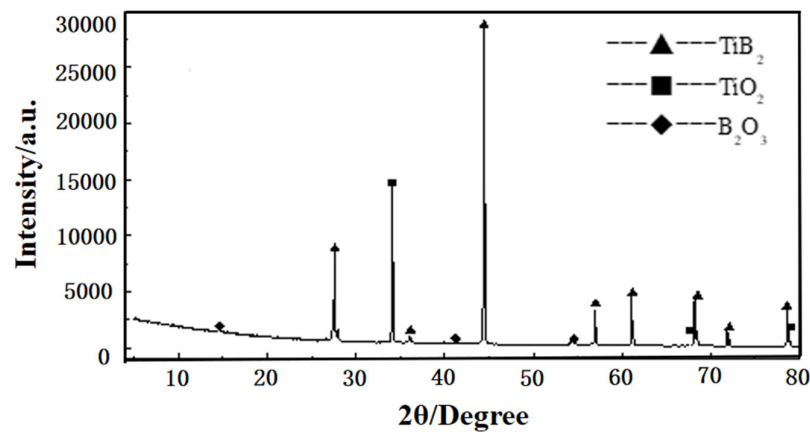


**Figure 3.** X-ray diffraction (XRD) patterns of plasma-sprayed  $\text{TiB}_2$  coating.

### 3.3. Wettability of $\text{TiB}_2$ Coating

Figure 4 compares the peeling of molten aluminum from two samples. Figure 4c shows that the liquid aluminum spreading on the surface of the carbon block cathode was easily peeled off from the substrate and will not peel off with the carbon block material. Figure 4d shows that it is desired to spread. It is very difficult for the liquid aluminum on the surface of the layer to peel off from the  $\text{TiB}_2$  substrate. The adhesion of the liquid aluminum to the coating is strong, and during the peeling of the coating, part of the coating materials peel off with the substrate; this also shows that the coating prepared by  $\text{TiB}_2$  inert cathode in this study has good wettability.

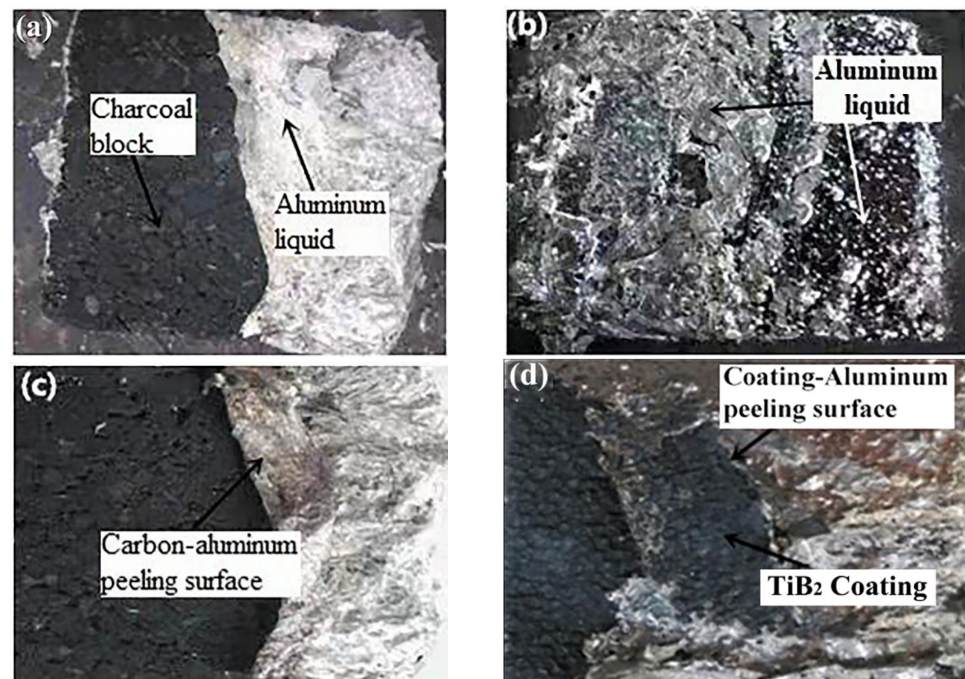


**Figure 4.** Characterization of wettability of  $\text{TiB}_2$  coating prepared using cathode carbon block and plasma spraying to liquid aluminum. (a) SEM image wetting effect diagram of cathode carbon block on molten aluminum, (b) SEM image wetting effect diagram of  $\text{TiB}_2$  coating on molten aluminum, and comparative characterization of wettability of liquid aluminum after peeling, (c) SEM image of the peeling of the molten aluminum from the cathode carbon block, (d) liquid aluminum peeling from  $\text{TiB}_2$  coating.

### 3.4. Corrosion Resistance of $TiB_2$ Coating Analysis of Solubility Loss of $TiB_2$ Coating in Molten Aluminum

Figure 5 depicts the change curve of the  $TiB_2$  coating prepared via plasma spraying in molten aluminum. The figure shows that the quality of the  $TiB_2$  coating remained unchanged and basically stable within 48 h of corrosion in high-temperature molten aluminum, demonstrating a good resistance to corrosion by molten aluminum. This is mainly because the  $TiB_2$  material had good wettability to liquid aluminum and low solubility in liquid aluminum. Moreover, the  $TiB_2$  coating prepared via plasma spraying was uniform and dense, demonstrating the good resistance of the  $TiB_2$  material to liquid aluminum erosion.

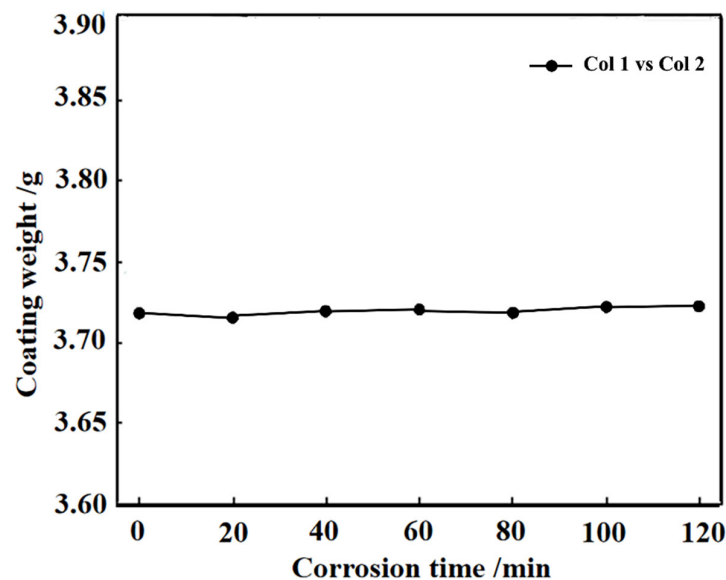


Figure 5. Variation curve of  $TiB_2$  coating quality with erosion time after aluminum alloy erosion.

According to the XRD analysis, after the  $TiB_2$  coating was corroded in high-temperature liquid aluminum (960 °C) for 120 min, no Ti component was detected, and the main component in the liquid aluminum was Al (Figure 6). The  $TiB_2$  coating prepared via plasma spraying could be well wetted by molten aluminum and had excellent corrosion resistance to molten aluminum. Moreover, the elemental analysis method was used to detect the Ti content in the molten aluminum. The Ti content of the molten aluminum was 0.0042%, which was only 0.0016% higher than that of the original aluminum (0.0026%). It was found that the titanium content in the original aluminum was 0.0026% (mass percent), and after the  $TiB_2$  coating was immersed in the aluminum solution for 48 h, the titanium content in the analyzed aluminum was 0.0042% (mass percent), which was only 0.0016% higher than the original aluminum content of 0.0026%. According to this calculation, the industrial tank was coated with 1 mm. The service life of thick pure  $TiB_2$  coating should be over four years.

### 3.5. Analysis of Static Corrosion Results of $TiB_2$ Coating

Resistance to Na penetration is an important indicator of wettable cathode materials. Figure 7a is a low-power-SEM image of the surface of the sample after the static corrosion of the carbon block, and Figure 7b is a low-power-SEM image of the  $TiB_2$  coating surface after static corrosion. The figure shows that after cryolite corrosion under the same conditions, the surface of the carbon block cathode was loose and porous, the area of the carbon block was significantly reduced, and the electrolyte was more likely to penetrate into the carbon block. Figure 8a is the surface micro-topography image of the  $TiB_2$  coating after corrosion, and Figure 8b is the cross-sectional micro-topography image of the  $TiB_2$  coating after corrosion. Figure 8a shows that after the coating surface was corroded, the  $TiB_2$  particles still maintained the original crystal structure state and were not corroded by cryolite melt.

Figure 8b shows that the  $\text{TiB}_2$  coating cross section also maintained the original complete structure; the coating structure was still dense. After 100 h of static corrosion, the  $\text{TiB}_2$  coating internal structure was dense, and the corrosion resistance was good. Figure 9 shows the EDS spectrum of the  $\text{TiB}_2$  coating after corrosion. The figure shows that the main component element in the coating was Ti, and the metal  $\text{Na}^+$  ions did not penetrate into the coating.

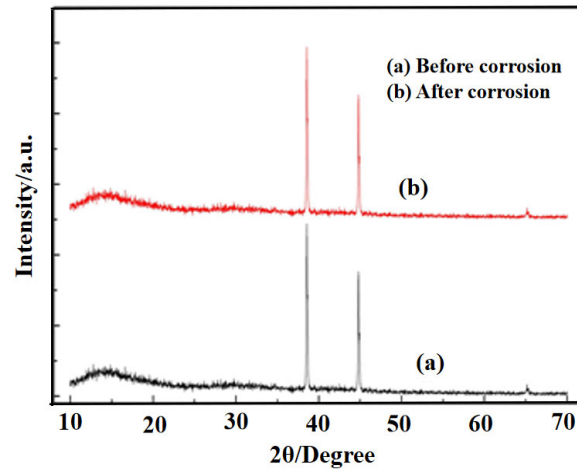


**Figure 6.** XRD analysis results of  $\text{TiB}_2$  coatings before and after erosion in liquid aluminum for around 120 min. (a) Before corrosion. (b) After corrosion.

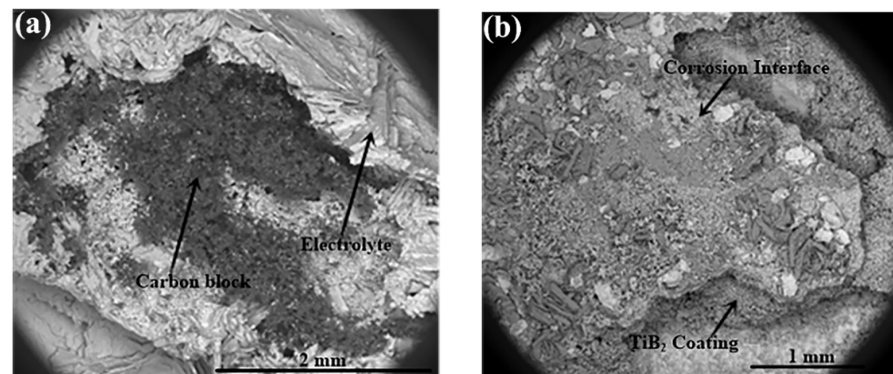


**Figure 7.** Charcoal surface and the coating surface after etching contrast. (a) Low magnification SEM image of sample surface after carbon block static corrosion, and (b) low magnification SEM image of  $\text{TiB}_2$  coating surface after static corrosion.

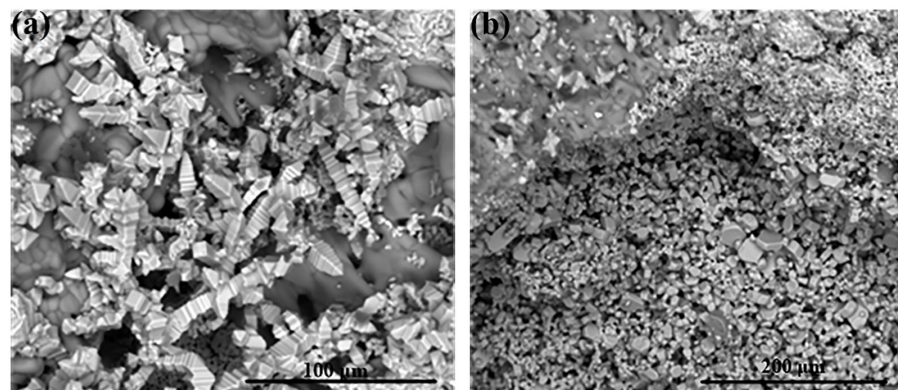


**Figure 8.** (a) Surface and (b) cross section after  $\text{TiB}_2$  coating corrosion.

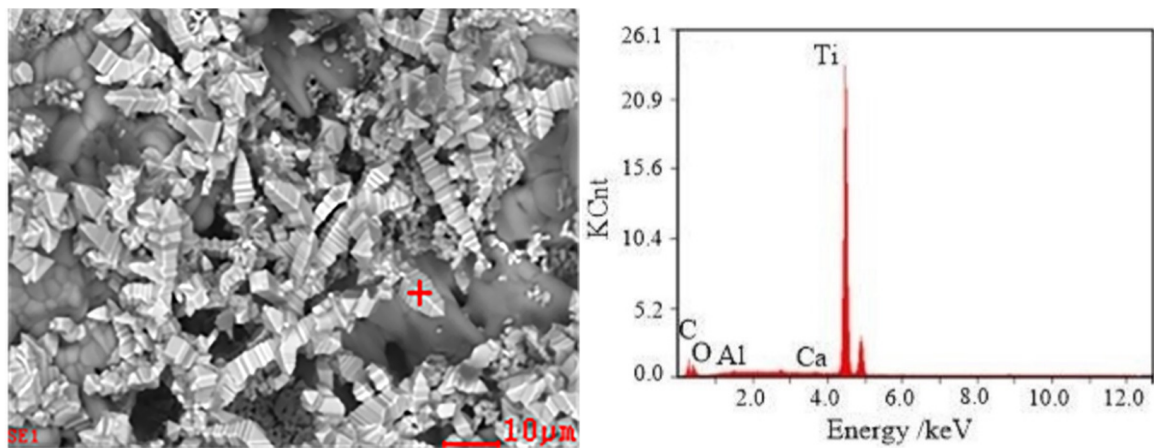


Figure 9. Energy-dispersive X-ray spectroscopy (EDS) analysis after corrosion of TiB<sub>2</sub> coating surface.

3.6. Analysis of Dynamic Corrosion Results of TiB<sub>2</sub> Coating

Figure 10 is a cross-sectional view of the TiB<sub>2</sub> coating after dynamic corrosion, and Figure 11 is the cross section of the TiB<sub>2</sub> coating after the dynamic corrosion experiment and the EDS energy spectrum of points taken near the TiB<sub>2</sub> coating surface.

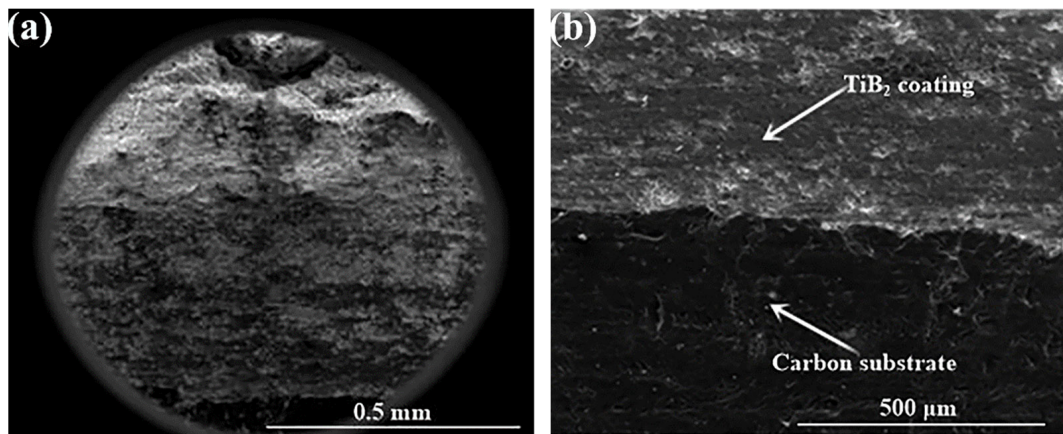


Figure 10. The section after the corrosion of the TiB<sub>2</sub> coating. (a) Low-magnification figure and (b) Micro-topography.

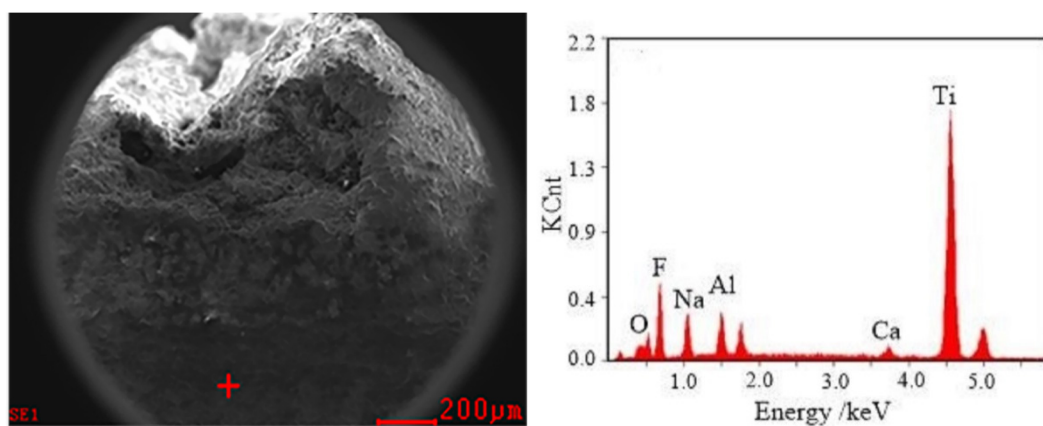


Figure 11. Cross section and EDS spectrum of coating after corrosion.

Figure 10a shows that the  $\text{TiB}_2$  coating after electrolysis maintained a compact structure. Figure 10b shows that the bonding surfaces of the  $\text{TiB}_2$  coating and the carbon block substrate were in good contact, without peeling or porosity of the coating. The  $\text{TiB}_2$  coating had good bonding strength with the carbon block substrate. From the analysis of the EDS results, a small amount of cryolite components such as F, Na, Al, and Ca occurred in this area. The main component of the coating was Ti; this indicates that a small amount of cryolite penetrated the coating surface after the electrolysis experiment; the penetration depth was not deep, indicating that the  $\text{TiB}_2$  coating obtained via plasma spraying has improved resistance to cryolite corrosion. The  $\text{TiB}_2$  wettable cathode coating prepared through plasma spraying technology does not contain carbon elements, which avoids the defect that the  $\text{TiB}_2/\text{C}$  carbon glue coating is easily corroded by the electrolyte due to carbon elements.

#### 4. Conclusions

In this study, under optimal parameters and the optimal particle size, a  $\text{TiB}_2$  coating was prepared on a carbon cathode surface using plasma-spraying equipment, and the phase and microstructure of the coating were analyzed via SEM, XRD, and other characterization methods. After the analysis, the wettability and corrosion resistance of the coating were measured, and the following conclusions were drawn:

The  $\text{TiB}_2$  coating prepared via APS had a smooth surface free of peeling and cracking. The  $\text{TiB}_2$  coating internal structure was dense and uniform. The large particles were in a semi-melted state, forming a disc-shaped structure embedded in the coating, and the small particles were completely melted; they connected the large particles to fill the pores between the large particles. In the plasma-spraying process, the air drawn into the plasma jet contacted the molten  $\text{TiB}_2$  particles, causing the  $\text{TiB}_2$  particles to be oxidized and form oxidation products such as  $\text{TiO}_2$  and  $\text{B}_2\text{O}_3$ .  $\text{TiB}_2$  is still the most important phase component in the coating.

The wettability between the  $\text{TiB}_2$  wettable cathode coating and molten aluminum was significantly better than that between graphite cathode carbon block and molten aluminum. Through static corrosion experiments, the abilities of the  $\text{TiB}_2$  coating and graphite cathode carbon block to resist Na penetration and to prevent molten cryolite corrosion were compared. The  $\text{TiB}_2$  coating resistance to Na penetration and corrosion resistance to molten cryolite were better than those of the graphite cathode carbon block. Moreover, after the  $\text{TiB}_2$  coating was dynamically corroded for 4 h, only a small amount of F, Na, and Al penetrated into the  $\text{TiB}_2$  coating inner surface. Given the results, the  $\text{TiB}_2$  coating prepared via plasma spraying has good liquid aluminum wetting ability and good resistance to Na penetration.

#### 5. Future Prospective

The oxidation behavior of  $\text{TiB}_2$  in the plasma spraying process is very complex, the process is very much influenced by the transfer (momentum transfer, heat transfer and mass transfer), especially the transfer phenomenon of gas phase  $\text{B}_2\text{O}_3$  under high temperature conditions determines the  $\text{TiB}_2$  oxidation behavior, and the plasma spraying  $\text{TiB}_2$  coating is carried out under high temperature conditions, and metallurgical bonding is observed through experiments, however, the bonding mechanism and the effect on  $\text{TiB}_2$  coating properties are still unclear; finally the introduction of multi-component  $\text{TiB}_2$  base can further improve the properties of the coating such as corrosion resistance and wettability. Therefore, on the basis of this thesis study, the following studies are proposed to be carried out in the future:

- (1) Study the momentum transfer, heat transfer and mass transfer behaviors of  $\text{TiB}_2$  during the movement to the surface of carbon block during the spraying process, analyze the time-varying laws of flow field and temperature field, and reveal the oxidation behavior of  $\text{TiB}_2$  and the symmetry mechanism of multi-physical field;

- and study in depth the mechanism of pore formation of TiB<sub>2</sub> coating under high temperature conditions and study the transfer phenomenon of gas phase B<sub>2</sub>O<sub>3</sub>.
- (2) To study the metallurgical bonding behavior of TiB<sub>2</sub> coating process for electrolytic aluminum by plasma spraying, to study the generation of new substances and formation of new chemical bonds by quantum chemical methods, and to reveal the possible chemical reactions by searching for transition states, and to propose the mechanism of the influence of metallurgical bonding on the performance of TiB<sub>2</sub> coating through the study.
  - (3) On the basis of TiB<sub>2</sub> coating research, we study multi-component TiB<sub>2</sub> based coating materials for aluminum electrolysis, add rare earth group elements to TiB<sub>2</sub> raw materials, study the mechanism of its addition on the performance of coating materials, and explore new high-performance TiB<sub>2</sub>-based coating materials for aluminum electrolysis.

**Author Contributions:** For research articles with several authors, Conceptualization, B.Y. and Y.H.; methodology, R.P.; validation, N.Y. and D.Z.; formal analysis, B.Y. and R.P.; investigation, Y.H.; resources, G.X.; writing—original draft preparation, B.Y.; writing—review and editing, B.Y.; supervision, Y.H.; funding acquisition, Y.H. and G.X. All authors have read and agreed to the published version of the manuscript.

**Funding:** This research received no external funding.

**Data Availability Statement:** Data sharing not applicable. No new data were created or analyzed in this study. Data sharing is not applicable to this article.

**Acknowledgments:** This work was financially supported by the National Natural Science Foundation of China (22168019, 52074141). The authors are grateful to NSFC, China for their support.

**Conflicts of Interest:** The authors declare no conflict of interest.

## References

1. Wang, X.; Leng, H.; Han, B.; Wang, X.; Hu, B.; Luo, H. Solidified microstructures and elastic modulus of hypo-eutectic and hyper-eutectic TiB<sub>2</sub>-reinforced high-modulus steel. *Acta Mater.* **2019**, *176*, 84–95. [[CrossRef](#)]
2. Kang, S.H.; Kim, D.J.; Kang, E.S.; Baek, S.S. Pressureless sintering and properties of titanium diboride ceramics containing chromium and iron. *J. Am. Ceram. Soc.* **2001**, *84*, 893–895. [[CrossRef](#)]
3. Lee, D.B.; Lee, Y.C.; Kim, D.J. The oxidation of TiB<sub>2</sub> ceramics containing Cr and Fe. *Oxid. Met.* **2001**, *56*, 177–189. [[CrossRef](#)]
4. Luo, X.; Wang, Z.; Hu, X.; Shi, Z.; Gao, B.; Wang, C.; Chen, G.; Tu, G. Influence of Metallic Additives on Densification Behaviour of Hot-Pressed TiB<sub>2</sub>. In *Light Metals*; The Minerals, Metals & Materials Society: Warrendale, PA, USA, 2009; pp. 1151–1155.
5. Liao, N.; Xu, L.; Jin, Y.; Xiao, Y.; Grasso, S.; Hu, C. Synthesis, microstructure, and mechanical properties of TiC-SiC-Ti<sub>3</sub>SiC<sub>2</sub> composites prepared by in situ reactive hot pressing. *Int. J. Appl. Ceram. Technol.* **2020**, *17*, 1601–1607. [[CrossRef](#)]
6. Liu, W.; Hao, C.-Y.; Zhao, X.-D.; Wang, X.-J.; Shi, G.-L. Strengthening mechanisms and tribological properties of ultra-hard AlMgB<sub>14</sub> based composite reinforced with TiB<sub>2</sub>. *Sci. Adv. Mater.* **2020**, *12*, 866–872. [[CrossRef](#)]
7. Fang, Z.; Wu, X.-L.; Yu, J.; Li, L.-B.; Zhu, J. Penetrative and migratory behavior of alkali metal in different binder based TiB<sub>2</sub>-C composite cathodes. *Trans. Nonferrous Met. Soc. China* **2014**, *24*, 1220–1230. [[CrossRef](#)]
8. Fan, X.; Huang, W.; Zhou, X.; Zou, B. Preparation and characterization of NiAl-TiC-TiB<sub>2</sub> intermetallic matrix composite coatings by atmospheric plasma spraying of SHS powders. *Ceram. Int.* **2020**, *46*, 10512–10520. [[CrossRef](#)]
9. Zhang, T.; Song, S.; Xie, C.; He, G.; Xing, B.; Li, R.; Zhen, Q. Preparation of highly-dense TiB<sub>2</sub> ceramic with excellent mechanical properties by spark plasma sintering using hexagonal TiB<sub>2</sub> plates. *Mater. Res. Express* **2019**, *6*, 125055. [[CrossRef](#)]
10. Islak, B.Y.; Candar, D. Synthesis and properties of TiB<sub>2</sub>/Ti<sub>3</sub>SiC<sub>2</sub> composites. *Ceram. Int.* **2021**, *47*, 1439–1446. [[CrossRef](#)]
11. Zhuang, W.; Yang, H.; Yang, W.; Cui, J.; Huang, L.; Wu, C.; Liu, J.; Sun, Y.; Meng, C. Microstructure, tensile properties, and wear resistance of in situ TiB<sub>2</sub>/6061 composites prepared by high energy ball milling and stir casting. *J. Mater. Eng. Perform.* **2021**, *30*, 7730–7740. [[CrossRef](#)]
12. Xiao, P.; Gao, Y.; Xu, F.; Yang, S.; Li, B.; Li, Y.; Huang, Z.; Zheng, Q. An investigation on grain refinement mechanism of TiB<sub>2</sub> particulate reinforced AZ91 composites and its effect on mechanical properties. *J. Alloys Compd.* **2019**, *780*, 237–244. [[CrossRef](#)]
13. Liu, J.H.; Blanpain, B.; Wollants, P. A XPS study of atmospheric plasma sprayed TiB<sub>2</sub> coatings. *Key Eng. Mater.* **2008**, *368–372*, 1347–1350. [[CrossRef](#)]
14. Gu, J.; Lee, S.-H.; Vu, V.H.; Yang, J.; Lee, H.-S.; Kim, J.-S. Fast fabrication of SiC particulate-reinforced SiC composites by modified PIP process using spark plasma sintering—Effects of green density and heating rate. *J. Eur. Ceram. Soc.* **2021**, *41*, 4037–4047. [[CrossRef](#)]

15. Wang, R.; Wang, S.; Li, D.; Xing, A.; Zhang, J.; Li, W.; Zhang, C. Theoretical characterization of the temperature dependence of the contact mechanical properties of the particulate-reinforced ultra-high temperature ceramic matrix composites in Hertzian contact. *Int. J. Solids Struct.* **2021**, *214–215*, 35–44. [[CrossRef](#)]
16. Song, B.; Yang, W.; Liu, X.; Chen, H.; Akhlaghi, M. Microstructural characterization of TiB<sub>2</sub>-SiC-BN ceramics prepared by hot pressing. *Ceram. Int.* **2021**, *47*, 29174–29182. [[CrossRef](#)]
17. Liu, Y.; Li, Z.; Peng, Y.; Huang, Y.; Huang, Z.; Zhang, D. Effect of sintering temperature and TiB<sub>2</sub> content on the grain size of B<sub>4</sub>C-TiB<sub>2</sub> composites. *Mater. Today Commun.* **2020**, *23*, 100875. [[CrossRef](#)]